CHEMISTRY OF MATERIALS

pubs.acs.org/cm

Article

Bromide Causes Facet-Selective Atomic Addition in Gold Nanorod Syntheses

Micah Brown and Benjamin J. Wiley*

Cite This: https://dx.doi.org/10.1021/acs.chemmater.0c01494

Read Online

ACCESS | Metrics & More | Article Recommendations | Supporting Information

ABSTRACT: The aspect ratio-dependent properties of gold nanorods are used in a variety of applications, but the cause of anisotropic nanorod growth remains unclear. Measurements utilizing single-crystal electrodes were collected to determine what additive(s) in pentatwinned gold nanorod syntheses are responsible for facet-selective atomic addition. With cetyltrimethylammonium in the absence of bromide, the rate of atomic addition to Au(100) and Au(111) single crystals was the same, and isotropic nanoparticles were produced. The addition of increasing concentrations of bromide suppressed the rate of atomic addition to Au(100) relative to Au(111) and increased the aspect ratio of gold nanorods. Bromide was a more effective passivator of Au(100) in the absence of cetyltrimethylammonium, indicating cetyltrimethylammonium does not cause facet-selective atomic addition. Cetyltrimethylammonium surfactant is still necessary for gold nanorod growth because it reduces the rate of gold ion reduction and stabilizes suspended nanoparticles against aggregation.

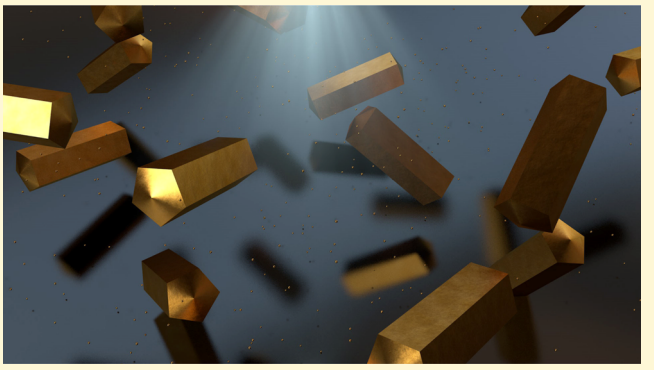

INTRODUCTION

The relationship between the aspect ratio and plasmonic properties of gold nanorods (AuNRs) has been harnessed for a variety of applications, including drug delivery,[1] catalysis,[2] surface-enhanced spectroscopies,[3] photothermal therapy,[4] and biomedical imaging.[5] Colloidal syntheses have proven a convenient and versatile means of AuNR production,[6] and improving their yield, uniformity, and scale has been a primary research objective.[7,8] Despite a number of mechanistic investigations, the underlying reason why AuNRs form remains unclear.[9−11] Understanding the facet-selective surface chemistry that leads to anisotropic atomic addition is fundamental to the design of optimized syntheses of metal nanostructures.

Gold nanorods can have single-crystal or pentatwinned crystal structures.[12] This study focuses on pentatwinned AuNRs because of the clear presentation of different facets at the AuNR tips and sides—{111} and {100}, respectively.[13,14] Pentatwinned AuNRs are typically grown in a two-step process: (1) synthesis of citrate-stabilized seeds (~3 nm in diameter) via reduction of chloroauric acid ($HAuCl_4$) with sodium borohydride, and (2) transfer of seeds to a growth solution in which $HAuCl_4$ is reduced by ascorbic acid (AA) in the presence of cetyltrimethylammonium bromide (CTAB).[15,16] The presence of bromide is essential for the growth of AuNRs, as the use of cetyltrimethylammonium chloride (CTAC) in place of CTAB yields isotropic nanoparticles.[17−20] The precise role of cetyltrimethylammonium cations (CTA^+) and bromide in driving anisotropic growth has been unclear. One hypothesis suggests that CTAB preferentially adsorbs to {100} facets on the sides of the nanocrystal, leading to preferential addition of Au to {111} facets.[21,22] Bromide increases the coadsorption of CTA^+ on Au surfaces, so facet-selective adsorption of bromide may lead to facet-selective adsorption of CTA^+.[12,23] Additionally, coordination of bromide and CTA^+ to gold ions can slow their reduction kinetics to potentially favor anisotropic growth.[7,24−26] In all, it has proven difficult to disentangle the individual effects of CTA^+ and bromide on both the surface chemistry of gold and the redox properties of the gold precursor.[27]

Metal nanocrystal growth often occurs through a process of atomic metal addition, which consists of a redox reaction between a reducing agent and metal precursor. These redox processes are readily observable under voltammetry, and the mixed potential theory allows the reaction rate (represented by the mixed potential current j_{MP}) to be extracted from voltammetric traces.[28] Rates of metal addition may then be compared across different growth solutions or, most critically, on different metal surfaces. Herein, we have aimed to model the facets of AuNRs through the use of single-crystal Au(111) and Au(100) electrodes. In effect, surface-mediated processes

Received: April 7, 2020
Revised: May 29, 2020
Published: June 1, 2020

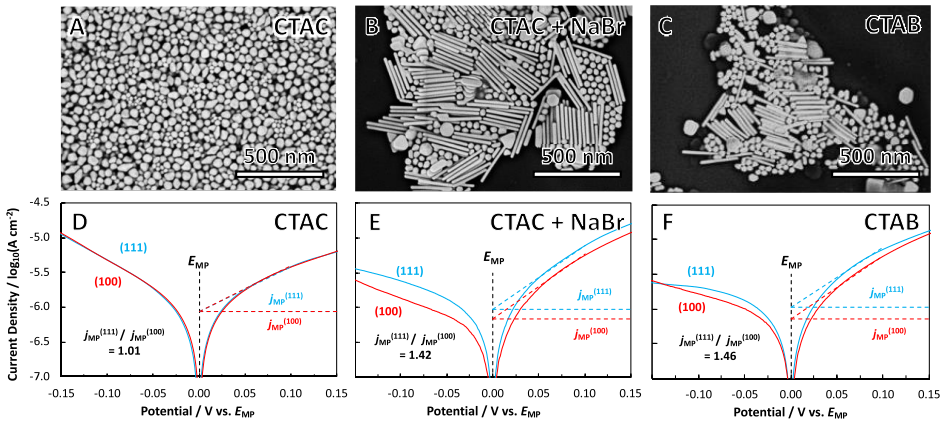

Figure 1. (A–C) SEM images of the synthesis product from seeded growth solutions containing 0.25 mM $HAuCl_4$, 0.55 mM AA, and either (A) 50 mM CTAC, (B) 50 mM CTAC and 50 mM NaBr, or (C) 50 mM CTAB. (D–F) Tafel plots collected on Au(111) and Au(100) single-crystal electrodes in seedless growth solutions containing 0.25 mM $HAuCl_4$, 0.55 mM AA, and either (D) 50 mM CTAC, (E) 50 mM CTAC and 50 mM NaBr, or (F) 50 mM CTAB. Traces were collected at 25 °C in a 0.2 M NaF background electrolyte no more than 20 s after AA injection (scan rate: 1 mV s^{-1}).

occurring on seed crystals at the nanoscale were magnified and observed as heterogeneous redox reactions on macroelectrodes.

The hypothesis that shape-directing additives preferentially adsorb to and modify the rate of atomic addition to certain metal facets has been tested with measurements collected on single-crystal electrodes.[28,29] Vivek and Burgess measured the adsorption of octyltrimethylammonium (OTA^+) and bromide on Au(100) and Au(111) single-crystal electrodes, finding that bromide shields OTA^+ from electrostatic repulsion at positive potentials, allowing coadsorption to occur.[23,30] However, they found no difference in the surface coverage of OTA^+ on Au(100) and Au(111) at a given surface charge density. The authors did not measure how adsorbates modify the rate of atomic addition.

This study reports for the first time how the presence of CTA^+ and bromide alter the rate of atomic addition to Au(111) and Au(100) electrodes. Our findings suggest that bromide alone is responsible for facet-selective atomic addition, while CTA^+ acts to slow the rate of gold ion reduction and stabilize nanoparticles against aggregation.

EXPERIMENTAL SECTION

Materials and Reagents. A polycrystalline Au electrode (3 mm dia.), glassy carbon electrode (3 mm dia.), silver–silver chloride (Ag|AgCl; 1 M KCl) reference electrode, mercury–mercurous sulfate ($Hg|Hg_2SO_4$; sat. K_2SO_4; SSE) reference electrode, and Pt counter electrode were obtained from CH Instruments (Austin, TX). Single-crystal Au(111) and Au(100) disks (3 mm dia.) were obtained from Princeton Scientific (Easton, PA) and mounted in an insulating poly(ether ether ketone) (PEEK) sheath for use as working electrodes. Electrical contact between the back of single crystals and a copper lead was made with silver epoxy. Hydrochloric acid (HCl), sulfuric acid (H_2SO_4), perchloric acid ($HClO_4$), sodium fluoride (NaF), and tetrachloroauric(III) acid trihydrate ($HAuCl_4 \cdot 3H_2O$, 99.99%) were obtained from Fisher Scientific (Hampton, NH). Hexadecyltrimethylammonium bromide (CTAB), hexadecyltrimethylammonium chloride (CTAC), sodium bromide (NaBr), ascorbic acid (AA), sodium borohydride ($NaBH_4$), sodium citrate dihydrate ($Na_3(Ci) \cdot 2H_2O$), and sodium hydroxide (NaOH) were obtained from Sigma Aldrich (St. Louis, MO). All reagents were used as received without further purification. Inductively coupled plasma mass spectrometry (ICP-MS) was used to quantify trace iodide in CTAB, CTAC, and NaBr reagents (Table S2), as concentrations exceeding 2.75 ppm may inhibit nanorod growth.[31]

Synthesis of Gold Nanorods. A standard two-step protocol using both seed and growth solutions was adopted.[13,16] For the seed solution, 1 mL of 10 mM sodium citrate, 10 mL of 1 mM $HAuCl_4$, and 28 mL of DI water were added to a 50 mL centrifuge tube. To this solution, 1 mL of ice-chilled 100 mM $NaBH_4$ was injected, initiating an immediate color change from faint yellow to dark red. The centrifuge tube was continually vortexed for 5 min immediately following $NaBH_4$ injection. The seed solution was left at room temperature (20 °C) for ~3 h to allow hydrolysis of remaining $NaBH_4$. AuNR growth solutions consisted of 0.25 mM $HAuCl_4$ and 50 mM CTAC or CTAB. Concentrations of NaBr were varied from 6.25 to 125 mM in growth solutions containing 50 mM CTAC. Scintillation vials containing 10.0 mL of growth solution were injected with 55 μL of 100 mM AA, changing the solution from yellow-orange to colorless. Finally, 10 μL of Au seed solution was injected to initiate nanoparticle growth. Solutions were stirred briefly and placed in a 25 °C water bath overnight (~18 h). Solutions were centrifuged twice (1500 rpm, 10 min) to remove excess capping agents and concentrate nanoparticles. Particle morphology was assessed by scanning electron microscopy (SEM) on a Thermo Fisher Scientific Apreo S SEM in the Shared Materials Instrumentation Facility at Duke University (Durham, NC).

Electrode Preparation. Electrochemical measurements were carried out on a CHI600D potentiostat (CH Instruments; Austin, TX). All potentials cited are with respect to the Ag|AgCl (1 M KCl) reference electrode unless otherwise noted. Before measurement, the surface of the working electrode was sequentially polished on a microfiber cloth with alumina slurries of particle diameter 1.0, 0.3, and 0.05 μm (Buehler; Lake Bluff, IL). Mechanically polished electrodes were then sonicated in ethanol for 30 s to dislodge impacted alumina, dried under a nitrogen stream, and electro-oxidized in a solution of chloride-free 0.1 M H_2SO_4 at 10 V vs a glassy carbon counter electrode for 20 s. The resulting brown overlayer of gold oxide was then dissolved in 1 M HCl, yielding well-ordered terraces on single-crystal electrodes.[32] As confirmation, single-crystal electrodes were transferred to a solution of 0.10 M $HClO_4$ and cycled between 0 and +1.4 V at a scan rate of 20 mV s^{-1}. Observation of facet-specific features for Au(111) or Au(100) in the +0.7 to +1.4 V region of the anodic sweep was used as assurance of proper surface preparation (Figure S1).[23,30,33]

Electrochemical Measurements. All solutions used for electrochemical analysis were prepared in 200 mM NaF supporting electrolyte. Growth solutions were prepared by dissolving metal precursor (0.25 mM $HAuCl_4$) in an electrolyte containing 50 mM CTAC, 50 mM CTAB, or no capping agent. The concentration of

https://dx.doi.org/10.1021/acs.chemmater.0c01494
Chem. Mater. XXXX, XXX, XXX–XXX

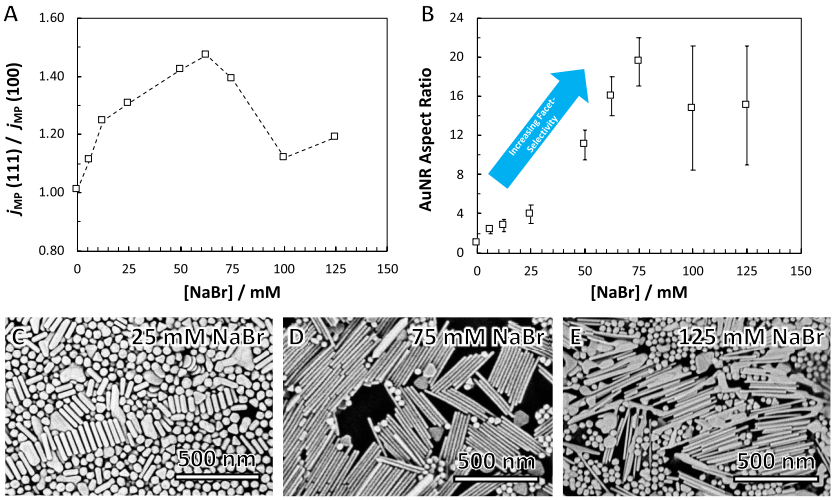

Figure 2. (A) Ratio of the currents at the mixed potential for Au(111) and Au(100) single-crystal electrodes as a function of bromide concentration in seedless growth solutions, which otherwise contained 0.25 mM $HAuCl_4$, 0.55 mM AA, and 50 mM CTAC. (B) Aspect ratio of gold nanorods grown with increasing bromide concentrations (other reagents the same as in (A)). (C–E) Representative SEM micrographs of select syntheses from (B).

NaBr was varied from 6.25 to 125 mM in solutions containing 50 mM CTAC. No seed solution was added to the growth solution for the electrochemical analyses. For a single measurement, 10 mL of a growth solution was added to a scintillation vial and placed in a 25 °C water bath. The three-electrode system (Au working, Ag|AgCl reference, and Pt counter electrodes) was immersed into the growth solution. After 5 min, 55 μL of 100 mM AA was injected into the solution, and a color change from yellow-orange to clear marked the reduction of Au(III) to Au(I). A linear sweep voltammogram (LSV) was collected from −0.2 to +0.2 V at a scan rate of 1 mV s^{-1} (400 s runtime), initiated no more than 20 s after AA injection. For kinetic analysis, 10 LSV traces were collected sequentially. Raw Tafel plots were generated from LSV traces by taking the logarithm of the current density (Figure S2), and plots were centered at the mixed potential (E_{MP}) for both Au(111) and Au(100) runs.

RESULTS AND DISCUSSION

Br^- but Not CTA^+ Selectively Passivates {100} Facets on Au. Several studies have demonstrated synthetically that bromide is necessary for AuNR growth.[16,18,19] These results have been reproduced herein, as depicted in Figure 1A–C. Citrate-stabilized gold seeds were introduced to growth solutions containing 0.25 mM $HAuCl_4$, 0.55 mM AA, and 50 mM CTAC, yielding isotropic gold nanoparticles (Figure 1A). Addition of 50 mM NaBr to the same growth solution resulted in AuNRs (Figure 1B), as did replacing CTAC with 50 mM CTAB (Figure 1C). The presence of semispherical polyhedra (~40 nm diameter) is typical in pentatwinned nanorod syntheses, whose yields are typically less than 30%.[8]

To determine if bromide induces AuNR growth by affecting facet-selective atomic addition, we performed linear sweep voltammetry (LSV) on single-crystal electrodes immersed in each growth solution to measure rates of addition. Unlike the growth solutions used in nanoparticle syntheses, no seeds were added to these solutions to avoid the spontaneous reduction of ionic gold precursor. In place of seeds, Au(111) and Au(100) electrodes modeled the facets present on pentatwinned Au seeds—allowing comparison of the gold surface structure's effects on the kinetics of atomic addition.

Gold nanorods grow via the spontaneous reduction of a gold ion precursor and oxidation of AA. The current density from these cathodic (j_{red}) and anodic (j_{ox}) half reactions must be equal and opposite to avoid charge accumulation, resulting in net zero current density ($j_{ox} = -j_{red}$). The electrochemical potential corresponding to net zero current density is referred to as the mixed potential, E_{MP}. Assuming one or both half reactions are kinetically limited, the redox process can be described by the Butler–Volmer equation, in which the current density for either half reaction at the mixed potential ($|j_{ox}| = |j_{red}| = j_{MP}$) can be extracted from a Tafel plot (log|j| vs E).[28] In the high overpotential regions of the Tafel plot (e.g., $|E - E_{MP}| \geq 50$ mV), log|j| depends linearly on E. From these regions, Tafel lines may be extrapolated back to E_{MP} to determine the value of j_{MP}. This current density is a measure of the reaction rate, and thus values of j_{MP} measured on Au(111) and Au(100) single-crystal electrodes allow direct comparison of the rates of atomic addition between {111} and {100} facets on the Au seed crystal.

In growth solutions containing 50 mM CTAC, no difference was observed between the j_{MP} values on Au(111) and Au(100) electrodes, indicating that the rate of Au^0 addition (i.e., the rate of reduction of gold ion precursor by AA) was the same on each surface (Figure 1D). This finding is consistent with the lack of anisotropic growth in CTAC syntheses (Figure 1A). With addition of 50 mM NaBr to the CTAC growth solution, the j_{MP} value measured on Au(111) was 42 ± 7% greater than on Au(100) (Figure 1E). Similarly, Au(111) exhibited a 46 ± 8% greater j_{MP} value than Au(100) in growth solutions containing 50 mM CTAB (Figure 1F). The j_{MP} values collected on Au(111) remained unchanged in each solution, but the j_{MP} values collected on Au(100) decreased in the presence of bromide relative to CTAC trials. These results suggest that facet-preferential atomic addition accounts in part for the anisotropic growth of AuNRs, and this selectivity is due to passivation of {100} facets by bromide. Furthermore, CTA^+ cations do not by themselves induce differential rates of atomic addition on these facets.

It is clear that the ratio of j_{MP} values on Au(111) and Au(100) electrodes indicates qualitatively if a certain growth solution will elicit anisotropic growth. However, the magnitude of this ratio does not directly equate to the aspect ratio observed for pentatwinned nanorods. The AuNRs synthesized in Figure 1B,C have aspect ratios of 12 ± 2, which would seem

https://dx.doi.org/10.1021/acs.chemmater.0c01494
Chem. Mater. XXXX, XXX, XXX–XXX

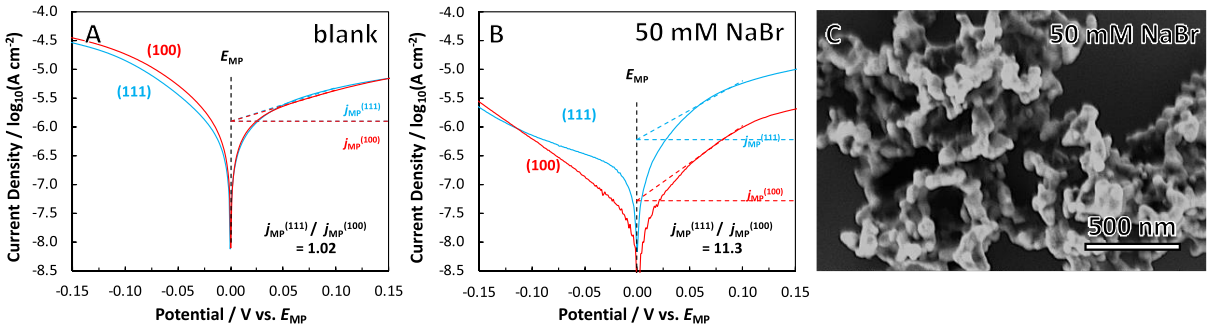

Figure 3. Tafel plots collected on Au(111) and Au(100) single-crystal electrodes in seedless growth solutions containing 0.25 mM $HAuCl_4$, 0.55 mM AA, 0.2 M NaF, (A) no additives, and (B) 50 mM NaBr. Traces were collected at 25 °C no more than 20 s after AA injection (scan rate: 1 mV s^{-1}). (B) Representative SEM micrograph of the Au^0 sediment produced from a seeded growth solution containing 0.25 mM $HAuCl_4$, 0.55 mM AA, and 50 mM NaBr.

to suggest that the rate of Au^0 addition is ca. 12-fold greater on Au(111) facets than on Au(100). In contrast, the ratio of j_{MP} values on Au(111) and Au(100) electrodes is 1.46. This apparent incongruity may be the result of a combination of factors, including surface adatom diffusion, inevitable surface defects on electrodes, and the fact that single-crystal macroelectrodes do not replicate the nearby edge sites that exist with facets on seed crystals.[28,30,34] Notably, the same electrochemical analysis was recently applied to pentatwinned copper nanowires with an aspect ratio ca. 100.[29] The copper nanowires are similarly bound by {100} facets at the nanocrystal sides and {111} facets at the tips. The j_{MP} ratio between these facets was approximately an order of magnitude larger than the values reported herein, which agrees with the greater degree of anisotropy for copper nanowires compared to AuNRs. Hence, though the j_{MP} ratio and aspect ratio do not necessarily match, the values do appear to trend together.

Effect of Br^- Concentration on Facet-Selective Current and Nanorod Aspect Ratio. To further investigate bromide's role in controlling AuNP anisotropy, increasing concentrations of NaBr (6.25−125 mM) were introduced into CTAC growth solutions for both synthetic and electrochemical experiments (Figures S3 and S4). With increasing bromide concentration, both the j_{MP} ratio and the average aspect ratio of the particles increased until a concentration of 75 mM (Figure 2). In this range, there is a consistent trend in the electrochemical and synthetic results, providing further evidence that bromide causes facet-selective atomic addition through passivation of {100} facets. Indeed, as the bromide concentration rose from 6.25 to 75 mM, the width of AuNRs decreased from 41 ± 4 to 18 ± 1 nm (Table S1). At NaBr concentrations greater than 75 mM, both the j_{MP} and average aspect ratio decreased (Figure 2A,B,E). The fall in both these values may then be attributed to bromide passivating {111} facets in addition to {100} at concentrations greater than ∼75 mM. This hypothesis is supported by the slightly shorter lengths and larger diameters of the gold nanorods produced at concentrations above 75 mM (Table S1). A {111} passivating effect at elevated bromide concentrations has been noted previously.[17]

Determining the Role of CTA^+. If CTA^+ is necessary for facet-selective atomic addition, then the suppression of the current on Au(100) electrodes would require its presence. Results from a control experiment (Figure 3A) show that the j_{MP} is the same for Au(111) and Au(100) electrodes in the absence of CTA^+ and NaBr. Upon addition of 50 mM NaBr, the j_{MP} is 11.3 times lower on Au(100) than Au(111). As the suppression of current on Au(100) is eight times greater without CTA^+ (compare with Figure 1E,F), we can conclude that bromide is the key driver of facet-selective atomic addition. However, growth solutions containing NaBr and no CTA^+ yielded an aggregated Au nanoparticle sediment (Figure 3B). Thus, while CTA^+ does not cause facet-selective atomic addition, it is still essential for the colloidal stabilization of Au seeds and the production of AuNRs.

It was clear from looking at the growth solutions that the presence of CTA^+ slowed the rate of gold particle formation. In growth solutions containing NaBr without CTA^+, addition of AA yielded visible Au^0 sediment within 10 min, whereas solutions containing CTAB remained clear (Figure 4). We

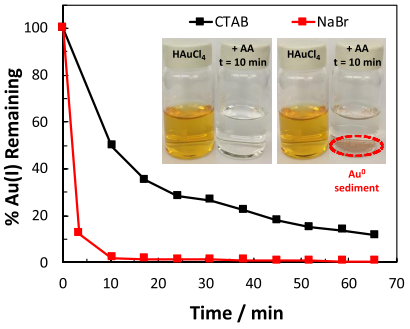

Figure 4. Electrochemical monitoring of the $HAuCl_4$ gold precursor concentration in situ as a function of time in growth solutions initially containing 0.25 mM $HAuCl_4$, 0.55 mM AA, and either (red) 50 mM NaBr or (black) 50 mM CTAB. Inset photographs depict these solutions before (yellow-orange) and 10 min after (clear) injection of AA.

developed an electrochemical method to directly monitor the consumption of ionic gold precursor in these growth solutions. LSV traces were collected in solutions containing either NaBr or CTAB with different concentrations of ionic gold (Figure S5A,B). Calibration curves were then generated from the cathodic currents at −0.18 V, a potential well below the onset of AA oxidation at +0.1 V (Figure S5C,D). Sequential LSV traces were then collected in growth solutions with and without CTA^+ after injection of AA over the course of ∼1 h (Figure S6), allowing us to monitor the amount of ionic gold vs time (Figure 4). In the absence of CTA^+, ionic gold is almost completely reduced by 10 min, whereas only half is consumed by this timepoint in the presence of CTA^+. After 1

https://dx.doi.org/10.1021/acs.chemmater.0c01494
Chem. Mater. XXXX, XXX, XXX−XXX

h, 12% of the initial ionic gold is still available for reduction in the CTAB solution, indicating that the presence of CTA^+ decreased the overall reaction rate ~20-fold. These results suggest that a necessary role of CTA^+ is to decrease the redox reaction rate between the AA and ionic gold precursor to a degree conducive for AuNR growth as well as prevent nanoparticle aggregation.

CONCLUSIONS

In summary, electrochemical measurements of the rate of atomic addition on Au(111) and Au(100) single-crystal electrodes indicate that bromide selectively passivates {100} facets on the sides of pentatwinned gold nanorods, leading to selective addition of gold to {111} facets on the ends of nanorods. Cetyltrimethylammonium cations do not induce facet-selective atomic addition by themselves and interfere with the ability of bromide to selectively passivate Au(100). We therefore conclude that cetyltrimethylammonium does not cause facet-selective atomic addition. However, cetyltrimethylammonium is still necessary for nanorod growth because it slows the reduction rate of ionic gold precursor and stabilizes colloidal nanoparticles, thereby preventing rapid precipitation of the Au^0 sediment from the growth solution. This work adds to the growing literature illustrating the ability of electrochemical methods to provide new insights into the roles of shape-directing additives in the syntheses of metal nanostructures.[28,29]

ASSOCIATED CONTENT

Supporting Information

The Supporting Information is available free of charge at https://pubs.acs.org/doi/10.1021/acs.chemmater.0c01494.

Additional description of the mixed potential theory analysis; cyclic voltammograms to confirm proper surface preparation; raw LSVs and Tafel plots; SEM micrographs of the products of various AuNR syntheses; LSVs and calibration curves for the measurement of ionic gold precursor concentration; gold nanorod dimensions with increasing NaBr concentration; iodide content of reagents as measured by ICP-MS (PDF)

AUTHOR INFORMATION

Corresponding Author

Benjamin J. Wiley − *Department of Chemistry, Duke University, Durham, North Carolina 27708, United States;* orcid.org/0000-0002-1314-6223; Email: benjamin.wiley@duke.edu

Author

Micah Brown − *Department of Chemistry, Duke University, Durham, North Carolina 27708, United States*

Complete contact information is available at: https://pubs.acs.org/10.1021/acs.chemmater.0c01494

Notes

The authors declare no competing financial interest.

ACKNOWLEDGMENTS

Funding for this research was provided by the National Science Foundation Grant No. CHE-1808108.

REFERENCES

(1) Pissuwan, D.; Valenzuela, S. M.; Cortie, M. B. Prospects for Gold Nanorod Particles in Diagnostic and Therapeutic Applications. *Biotechnol. Genet. Eng. Rev.* **2008**, *25*, 93−112.

(2) Han, C.; Qi, M.-Y.; Tang, Z.-R.; Gong, J.; Xu, Y.-J. Gold nanorods-based hybrids with tailored structures for photoredox catalysis: fundamental science, materials design and applications. *Nano Today* **2019**, *27*, 48−72.

(3) Nikoobakht, B.; El-Sayed, M. A. Surface-Enhanced Raman Scattering Studies on Aggregated Gold Nanorods. *J. Phys. Chem. A* **2003**, *107*, 3372−3378.

(4) Pérez-Juste, J.; Pastoriza-Santos, I.; Liz-Marzán, L. M.; Mulvaney, P. Gold nanorods: Synthesis, characterization and applications. *Coord. Chem. Rev.* **2005**, *249*, 1870−1901.

(5) Elahi, N.; Kamali, M.; Baghersad, M. H. Recent biomedical applications of gold nanoparticles: A review. *Talanta* **2018**, *184*, 537−556.

(6) Jana, N. R.; Gearheart, L.; Murphy, C. J. Wet Chemical Synthesis of High Aspect Ratio Cylindrical Gold Nanorods. *J. Phys. Chem. B* **2001**, *105*, 4065−4067.

(7) Huo, D.; Kim, M. J.; Lyu, Z.; Shi, Y.; Wiley, B. J.; Xia, Y. One-Dimensional Metal Nanostructures: From Colloidal Syntheses to Applications. *Chem. Rev.* **2019**, *119*, 8972−9073.

(8) Scarabelli, L.; Sánchez-Iglesias, A.; Pérez-Juste, J.; Liz-Marzán, L. M. A "Tips and Tricks" Practical Guide to the Synthesis of Gold Nanorods. *J. Phys. Chem. Lett.* **2015**, *6*, 4270−4279.

(9) Burrows, N. D.; Harvey, S.; Idesis, F. A.; Murphy, C. J. Understanding the Seed-Mediated Growth of Gold Nanorods through a Fractional Factorial Design of Experiments. *Langmuir* **2017**, *33*, 1891−1907.

(10) Lohse, S. E.; Murphy, C. J. The Quest for Shape Control: A History of Gold Nanorod Synthesis. *Chem. Mater.* **2013**, *25*, 1250−1261.

(11) Langille, M. R.; Personick, M. L.; Zhang, J.; Mirkin, C. A. Defining Rules for the Shape Evolution of Gold Nanoparticles. *J. Am. Chem. Soc.* **2012**, *134*, 14542−14554.

(12) Grzelczak, M.; Pérez-Juste, J.; Mulvaney, P.; Liz-Marzán, L. M. Shape control in gold nanoparticle synthesis. *Chem. Soc. Rev.* **2008**, *37*, 1783−1791.

(13) Johnson, C. J.; Dujardin, E.; Davis, S. A.; Murphy, C. J.; Mann, S. Growth and form of gold nanorods prepared by seed-mediated, surfactant-directed synthesis. *J. Mater. Chem.* **2002**, *12*, 1765−1770.

(14) Walsh, M. J.; Tong, W.; Katz-Boon, H.; Mulvaney, P.; Etheridge, J.; Funston, A. M. A Mechanism for Symmetry Breaking and Shape Control in Single-Crystal Gold Nanorods. *Acc. Chem. Res.* **2017**, *50*, 2925−2935.

(15) Jana, N. R.; Gearheart, L.; Murphy, C. J. Seed-Mediated Growth Approach for Shape-Controlled Synthesis of Spheroidal and Rod-like Gold Nanoparticles Using a Surfactant Template. *Adv. Mater.* **2001**, *13*, 1389−1393.

(16) DuChene, J. S.; Niu, W.; Abendroth, J. M.; Sun, Q.; Zhao, W.; Huo, F.; Wei, W. D. Halide Anions as Shape-Directing Agents for Obtaining High-Quality Anisotropic Gold Nanostructures. *Chem. Mater.* **2013**, *25*, 1392−1399.

(17) Si, S.; Leduc, C.; Delville, M.-H.; Lounis, B. Short Gold Nanorod Growth Revisited: The Critical Role of the Bromide Counterion. *ChemPhysChem* **2012**, *13*, 193−202.

(18) Sau, T. K.; Murphy, C. J. Role of ions in the colloidal synthesis of gold nanowires. *Philos. Mag.* **2007**, *87*, 2143−2158.

(19) Garg, N.; Scholl, C.; Mohanty, A.; Jin, R. The Role of Bromide Ions in Seeding Growth of Au Nanorods. *Langmuir* **2010**, *26*, 10271−10276.

(20) Murphy, C. J.; Thompson, L. B.; Alkilany, A. M.; Sisco, P. N.; Boulos, S. P.; Sivapalan, S. T.; Yang, J. A.; Chernak, D. J.; Huang, J. The Many Faces of Gold Nanorods. *J. Phys. Chem. Lett.* **2010**, *1*, 2867−2875.

(21) Meena, S. K.; Sulpizi, M. Understanding the Microscopic Origin of Gold Nanoparticle Anisotropic Growth from Molecular Dynamics Simulations. *Langmuir* **2013**, *29*, 14954−14961.

(22) Meena, S. K.; Celiksoy, S.; Schäfer, P.; Henkel, A.; Sönnichsen, C.; Sulpizi, M. The role of halide ions in the anisotropic growth of gold nanoparticles: a microscopic, atomistic perspective. *Phys. Chem. Chem. Phys.* **2016**, *18*, 13246−13254.
(23) Vivek, J. P.; Burgess, I. J. Quaternary Ammonium Bromide Surfactant Adsorption on Low-Index Surfaces of Gold. 1. Au(111). *Langmuir* **2012**, *28*, 5031−5039.
(24) Huang, M. H.; Chiu, C.-Y. Achieving polyhedral nanocrystal growth with systematic shape control. *J. Mater. Chem. A* **2013**, *1*, 8081−8092.
(25) Bullen, C.; Zijlstra, P.; Bakker, E.; Gu, M.; Raston, C. Chemical Kinetics of Gold Nanorod Growth in Aqueous CTAB Solutions. *Cryst. Growth Des.* **2011**, *11*, 3375−3380.
(26) Xia, Y.; Xia, X.; Peng, H.-C. Shape-Controlled Synthesis of Colloidal Metal Nanocrystals: Thermodynamic versus Kinetic Products. *J. Am. Chem. Soc.* **2015**, *137*, 7947−7966.
(27) Lohse, S. E.; Burrows, N. D.; Scarabelli, L.; Liz-Marzán, L. M.; Murphy, C. J. Anisotropic Noble Metal Nanocrystal Growth: The Role of Halides. *Chem. Mater.* **2014**, *26*, 34−43.
(28) Kim, M. J.; Brown, M.; Wiley, B. J. Electrochemical investigations of metal nanostructure growth with single crystals. *Nanoscale* **2019**, *11*, 21709−21723.
(29) Kim, M. J.; Alvarez, S.; Chen, Z.; Fichthorn, K. A.; Wiley, B. J. Single-Crystal Electrochemistry Reveals Why Metal Nanowires Grow. *J. Am. Chem. Soc.* **2018**, *140*, 14740−14746.
(30) Vivek, J. P.; Burgess, I. J. Quaternary Ammonium Bromide Surfactant Adsorption on Low-Index Surfaces of Gold. 2. Au(100) and the Role of Crystallographic-Dependent Adsorption in the Formation of Anisotropic Nanoparticles. *Langmuir* **2012**, *28*, 5040−5047.
(31) Smith, D. K.; Miller, N. R.; Korgel, B. A. Iodide in CTAB Prevents Gold Nanorod Formation. *Langmuir* **2009**, *25*, 9518−9524.
(32) Kibler, L. A. Preparation and characterization of noble metal single crystal electrode surfaces. *Int. Soc. Electrochem.* **2003**, 1−55.
(33) Hamelin, A. The crystallographic orientation of gold surfaces at the gold-aqueous solution interphases. *J. Electroanal. Chem. Interfacial Electrochem.* **1982**, *142*, 299−316.
(34) Hoogvliet, J. C.; Dijksma, M.; Kamp, B.; van Bennekom, W. P. Electrochemical Pretreatment of Polycrystalline Gold Electrodes To Produce a Reproducible Surface Roughness for Self-Assembly: A Study in Phosphate Buffer pH 7.4. *Anal. Chem.* **2000**, *72*, 2016−2021.

https://dx.doi.org/10.1021/acs.chemmater.0c01494
Chem. Mater. XXXX, XXX, XXX−XXX